D4.2 Report on fracture energy of the cell interconnect interface with the different chemical compositions and particle sizes measured at initial operation and after 3000 h of aging

PROJECT INFORMATION

GRANT AGREEMENT NUMBER	826323
PROJECT FULL TITLE	Low Cost Interconnects with highly improved Contact Strength for SOC Applications
PROJECT ACRONYM	LOWCOST-IC
FUNDING SCHEME	FCH-JU2
START DATE OF THE PROJECT	1/1-2019
DURATION	36 months
CALL IDENTIFIER	H2020-JTI-FCH-2018-1
PROJECT WEBSITE	www.lowcost-ic.eu

DELIVERABLE INFORMATION

WP NO.	4
WP LEADER	Ragnar Kiebach
CONTRIBUTING PARTNERS	DTU
NATURE	Report
AUTHORS	Peyman Khajavi, Yousef Alizad Farzin, Belma Talic, Ragnar Kiebach, Henrik Lund Frandsen
CONTRIBUTORS	
CONTRACTUAL DEADLINE	31/12/2019
DELIVERY DATE TO EC	31/08/2020

DISSEMINATION LEVEL

PU	Public	X
PP	Restricted to other programme participants (incl. Commission Services)	
RE	Restricted to a group specified by the consortium (incl. Commission Services)	
CO	Confidential, only for the members of the consortium (incl. Commission Services)	

1 Introduction

This is the first version of this deliverable prepared for the midterm evaluation. The experimental work has not been possible to finalize during the COVID 19 pandemic. Once the final experiments have been completed, the deliverable will be updated with all results.

Stacking of solid oxide cells (SOC) requires that a robust and durable electrical contact between the cell and the interconnect is established. To achieve this, contact layers are applied during the cell fabrication process or the stack assembly. The high electrical conductivity and good compatibility with the SOC oxygen electrode material makes the perovskite oxides as a most promising contact material in current state-of-the-art SOC stacks. However, sintering of these materials requires high temperature (> 1000 °C), which is not compatible with the other SOC stack components such as the steel interconnect and the glass(-ceramic) sealant. Thus these are either sintered ex-situ with poor contacting (no bonding) as a result, or in-situ with sintering at a lower temperature. The latter also results in an interface between the contact layer and the interconnect due to the low strength of the contact layer. Thus this interface is among the weakest in the stack and the one most prone to mechanical failure.

In the LOWCOST-IC project, we have investigated a novel contact layer solution based on the concept of reactive oxidative bonding. In this method, the contact layer is applied in the form of metal particles that during SOC stack operation (700-800°C) are oxidized *in-situ* to form dense and well-conducting oxides. The concept is illustrated in Figure 1. The metallic precursors investigated are Mn-Co and Mn-Cu, mixed in the stoichiometric ratios to form $MnCo_2O_4$ and $Cu_{1.3}Mn_{1.7}O_4$, respectively.

The compositions were chosen as both oxides have an appreciable electrical conductivity (70 and 225 S/cm at 750 °C, respectively) and a TEC (14.4 and 12.2 K^{-1} between 25 °C and 800 °C, respectively) matching other typically used SOC materials [1,2]. Due to the high reactivity of the metallic precursors during the oxidation, a strong bond is created to both the coated interconnect and the air electrode [3].

In order to validate this contact layer solution, the fracture toughness of the contact layer/interconnect interface has been measured by four-point bending. To investigate the long-term stability of the relevant interface the fracture toughness was evaluated after aging at 750°C and 850 °C, representing the average operating temperature for the stack of SOLIDpower and Sunfire, respectively. Post-test SEM and EDS analysis are used as a tool to determine where the crack propagates, i.e. which layer or interface is the weakest.

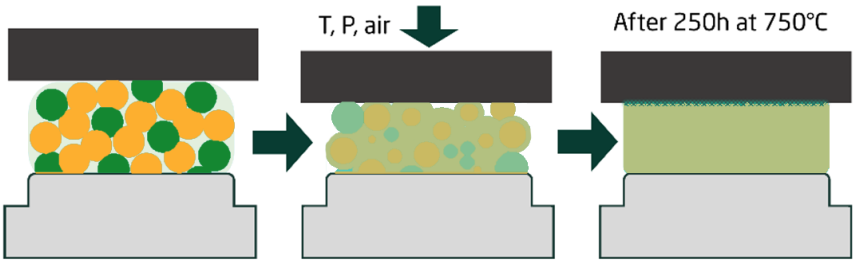

Figure 1. Schematic illustration of the reactive oxidative bonding concept for the fabrication of more robust contact layers

2 Materials and methods

The adhesion of the contact layer to the steel interconnect was evaluated by measuring the critical energy release rate (G_c) for crack generation, here also referred to as fracture energy. The fracture energy was evaluated by four-point bending following the method derived by Charalambides et al. [1] and modified by Hofinger et al. [2]. Details about the measurement method and the calculation of the fracture toughness based on the load measured from the four-point bending test can be found in [3,4]. An illustration of the samples used in the measurement is shown in figure 2.

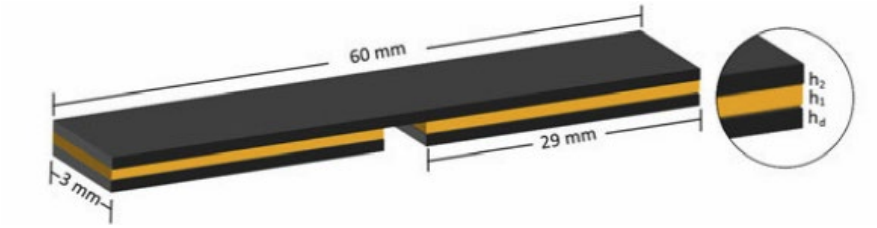

Figure 2. Illustration of the sandwiched sample used for the four-point bending test.

The two ferritic stainless bars of steel AISI 441 (Sandvik) and K44M (Aperam) in 0.3 mm thickness served as the interconnect material. The elemental content for the 441 and K44M stainless steels are summarized in table 1, where Cr content of the K44M slightly higher than 441 steel. The steels were tested both without any coating and coated with CeCo (Sandvik Materials). The CeCo coating on the 441 steel was produced on the production line while the CeCo coating on the K44M was produced with the batch coater. The steel was etched to make the two short bars (29 x 3 mm) and one long bar (60 x 3 mm) illustrated in Figure 2.

Table 1. Composition of steels

Steel	C	Si	Mn	P	S	Cr	Ti	Nb	N	Mo
441	0.03	1.00	1.00	0.04	0.015	17.5-18.5	0.10-0.6	3C + (0.3-1.00)		-
K44M	0.015	0.40	0.30	-	-	19.0	-	0.6	0.015	1.9

Two different contact layers, Mn-Co and Mn-Cu spinel oxide, were screen printed onto the shorter (29 x 3 mm^2) bars with a green thickness of ca. 0.2 mm. The pastes for screen printing were prepared using Mn (American Elements, 99.9 %, APS ~ 2 µm), Co (Thermo Fisher, 99.8 %, APS ~ 1.6 µm) and Cu (Thermo Fisher, 99 %, APS ~ 2-3.5 µm) metal powders, and a proprietary solvent + binder system developed at DTU. The powders were added in the stoichiometric amounts to upon oxidation form $MnCo_2O_4$ and $Cu_{1.3}Mn_{1.7}O_4$, respectively. The paste was dried at 90 °C for 1 h after screen printing, to evaporate the solvent before assembly.

The sandwiches were assembled/bonded by hot pressing to simulate the assembly of a SOC stack. For this purpose, the sandwiched sample was placed between two alumina plates, and a load of 16.7 N/cm^2 was put on top, mimicking the load applied during stack assembly. The loaded sandwich was gradually heated up to 800 °C following a sintering profile representative of SOC stack assembly conditions. This involved 2 dwelling at 600°C and 800°C, each for 1 h. A heating and cooling rate of 100 °C/h was used during the heat-treatment. From here on, this heat treatment is referred to as "sintering".

Following the sintering treatment, some samples were additionally aged at 750°C or 850°C for 250 h in the air (120°C/h heating and cooling rates). No load was applied during this heat treatment. An overview of all samples tested and their pre-treatments is given in Table 1. All four-point bending tests were performed at room temperature.

Table 2. Overview of samples tested and pre-treatment conditions

Sample assembly		Pre-treatment		
Substrate	Contact layer	Sintered	750 °C	850 °C
441	Co-Mn	X		
441	Cu-Mn	X		
441-CeCo	Co-Mn	X	X	X
441-CeCo	Cu-Mn	X	X	X
K44M	Co-Mn	X		
K44M	Cu-Mn	X		
K44M-CeCo	Co-Mn	X		
K44M-CeCo	Cu-Mn	X		

After the four-point bending test, the fractured sandwiches were manually disassembled to inspect the fracture surface by SEM and EDS (Hitachi TM-3000). The purpose of these investigations was to identify the layer and/or interface through which the cracks had propagated. Additional compositional analysis of the sample surface was done with X-ray diffraction in order to identify the phases formed after sintering and after aging at 750°C or 850°C.

3 Results

3.1 Fracture energy

Figure 3 shows a representative load-displacement curve recorded during the four-point bending test. A linear elastic loading (Load) is seen initially. At 2.4 N the crack starts to propagate and a sawtooth-shaped response is observed. This corresponds to a "softening" of the sample, as the crack makes it more compliant. From the level of the plateau of the top of the saw teeth, the fracture energy for the crack propagation in the specific interface can be evaluated [3,4].

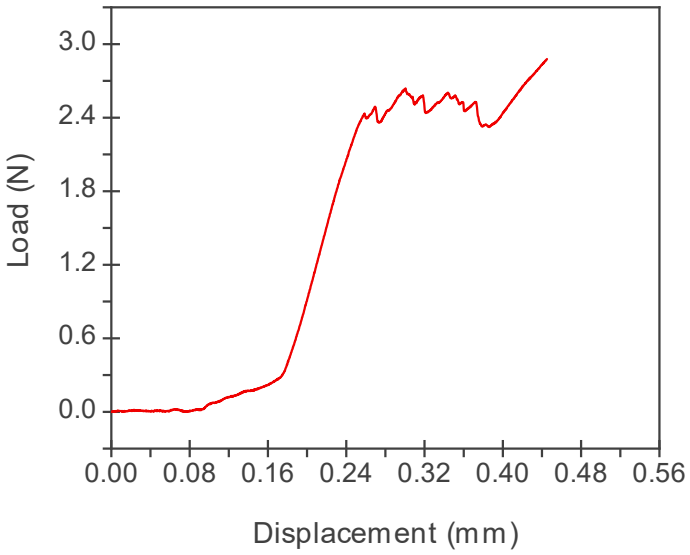

Figure 3. Representative load-displacement curve recorded during four-point bending

Fracture energies obtained for different contact layer/interconnect materials, as-sintered and after aging, are shown in Figure 4. For the as-sintered samples, the fracture energies for Co-Mn and Cu-Mn based contact layers deposited on the four types of interconnects (steel 441 and K44M, coated and uncoated) are presented. For both materials, the contact layer is more robust when deposited on the CoCe coated steel 441. The highest fracture energy is observed in the Cu-Mn spinel deposited on the CoCe coated steel 441 (i.e. 11.6 J/m^2). The fracture energy of Cu-Mn contact layer increases by aging: the samples aged for 250 h at 750 and 850 °C have fracture energy of 15.7 and 19.4 J/m^2, respectively. This is approximately 35% and 65% higher than the fracture energy of the as-sintered

samples. On the other hand, the fracture energy of Co-Mn samples decreases by aging. An analysis of this will be given once all other results have been presented in the following.

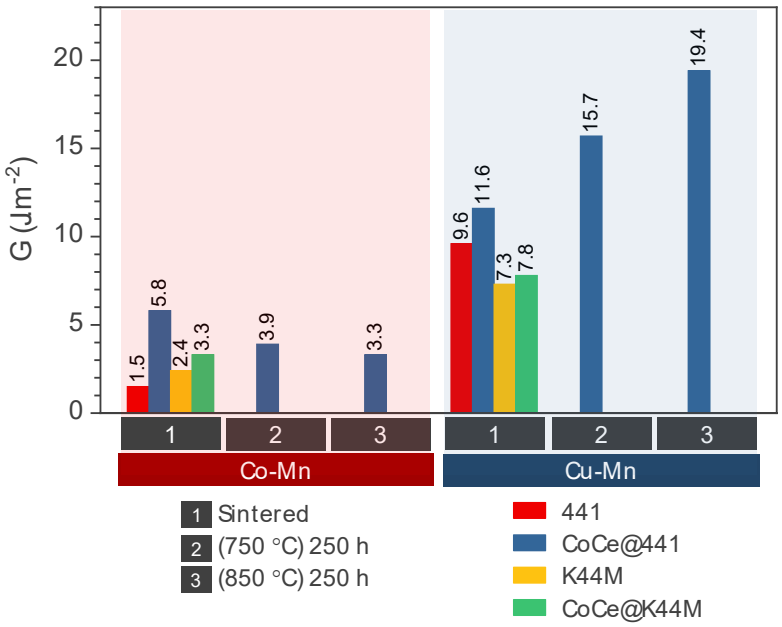

Figure 4. Fracture toughness of various interfaces

3.2 XRD analysis of contact layers

The XRD patterns of Co-Mn and Cu-Mn based samples, as-sintered and after aging experiments, are shown in Figure 5. The as-sintered Co-Mn sample contains 3 major phases, $CoMn_2O_4$, Co_2MnO_4, and Co_3O_4. The crystalline phase composition of the sample changes significantly during aging, as a result of reaction among different phases in the as-sintered samples and diffusion of Cr from interconnects. The sample aged at 850 °C for 250 h contains $MnCrCoO_4$, $MnCrO_4$ and $Cr_{1.3}Fe_{0.7}O_3$.

A similar trend is seen in the Cu-Mn based sample. The as-sintered Cu-Mn oxide consists of $Cu_{1.2}Mn_{1.8}O_4$, CuO, Cu_2O, Mn_3O_4, and Cu. After aging at 750°C, the $Cu_{1.2}Mn_{1.8}O_4$ and CuO phases are found in the sample. The observed Cu in the as-sintered samples can probably form a protective CuO layer on the substrate during aging. Increasing the aging temperature to 850 °C results in the formation of some $MnCrO_4$ and Fe_2O_3. The desired phases do thus need some time to appear, but as shown in Deliverable 4.1, a good conductivity (low ASR) of the contact layers is achieved immediately after assembly.

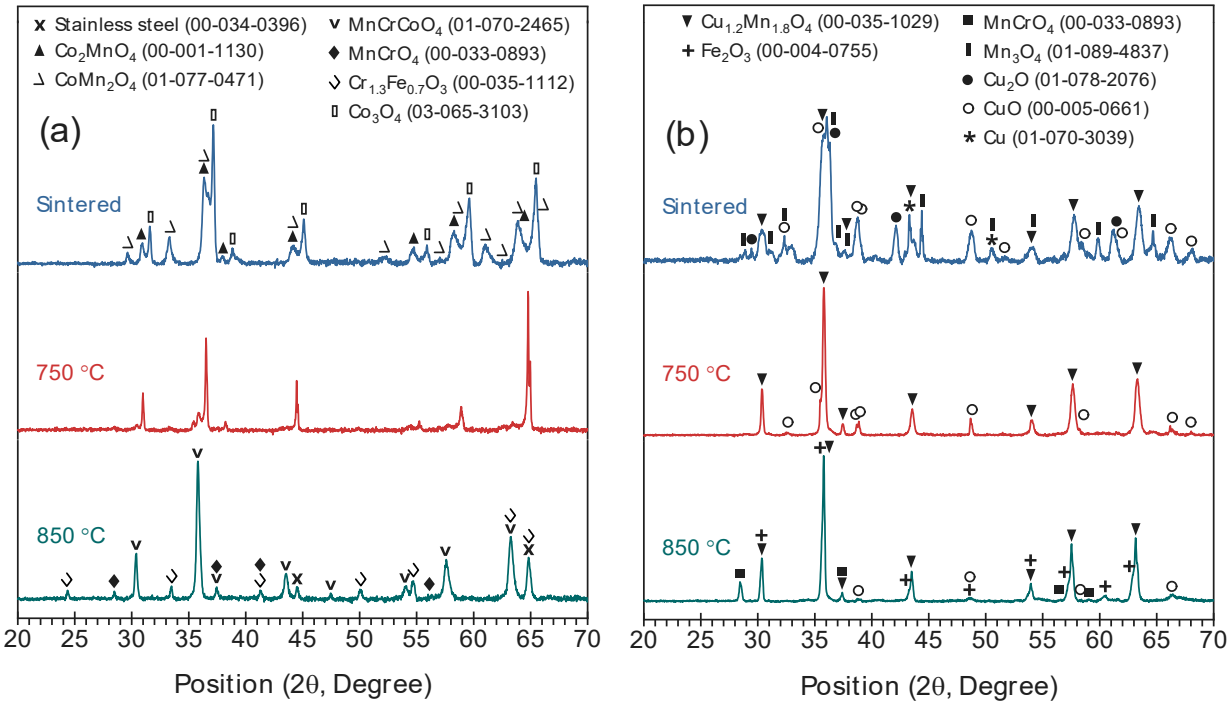

Figure 5. XRD patterns of (a) Co-Mn, and (b) Cu-Mn oxides, as-sintered and after aging at 750 and 850 °C for 250 h.

3.3 Post-fracture SEM and EDS analysis

The SEM/EDX analysis of the fractured surfaces of Co-Mn and Cu-Mn based samples are shown in Figure 6. As seen, the fractured surfaces contain the elements for both the contact layer and the oxide layer (Cr scale and/or Cr-Fe perovskite). It is hence conclude that the crack propagation has partly occurred through the interconnect layer, and partly through the oxide layer.

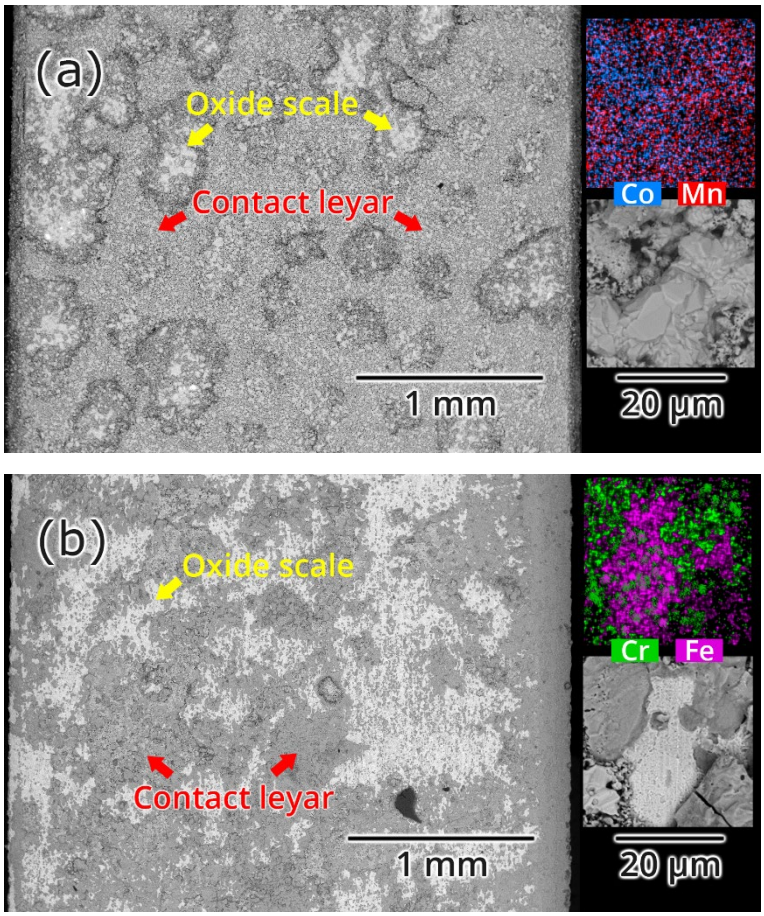

Figure 6. SEM micrographs of fractured surface of (a) Co-Mn oxide, and (b) Cu-Mn oxides samples aged at 850 °C for 250 hours.

The higher magnification SEM images (Figure 7) show a closer look at the microstructure of Co-Mn samples, as-sintered and after aging. The as-sintered sample contains big particles (7-20 µm) surrounded by small particles of 1 µm. After aging, the particle growth is observed as expected. Nevertheless, the microstructure of the aged samples shows the presence of small particles having a size of around 500 nm. The small particles in the aged samples are most probably $MnCrO_4$ formed by Mn (segregated from Mn-Co oxide) and Cr (diffused from the substrate) cations.

SEM images of Cu-Mn samples (Figure 8) show the higher density of the sample compared to the Co-Mn sample. The EDS results on both samples show that the Cr content significantly increases by increasing the aging time. This can be explained by the diffusion of Cr from the substrate. In addition, compared to the as-sintered samples and samples aged at 750 °C, a homogenous distribution of Mn and Co cations is observed in samples aged at 850°C.

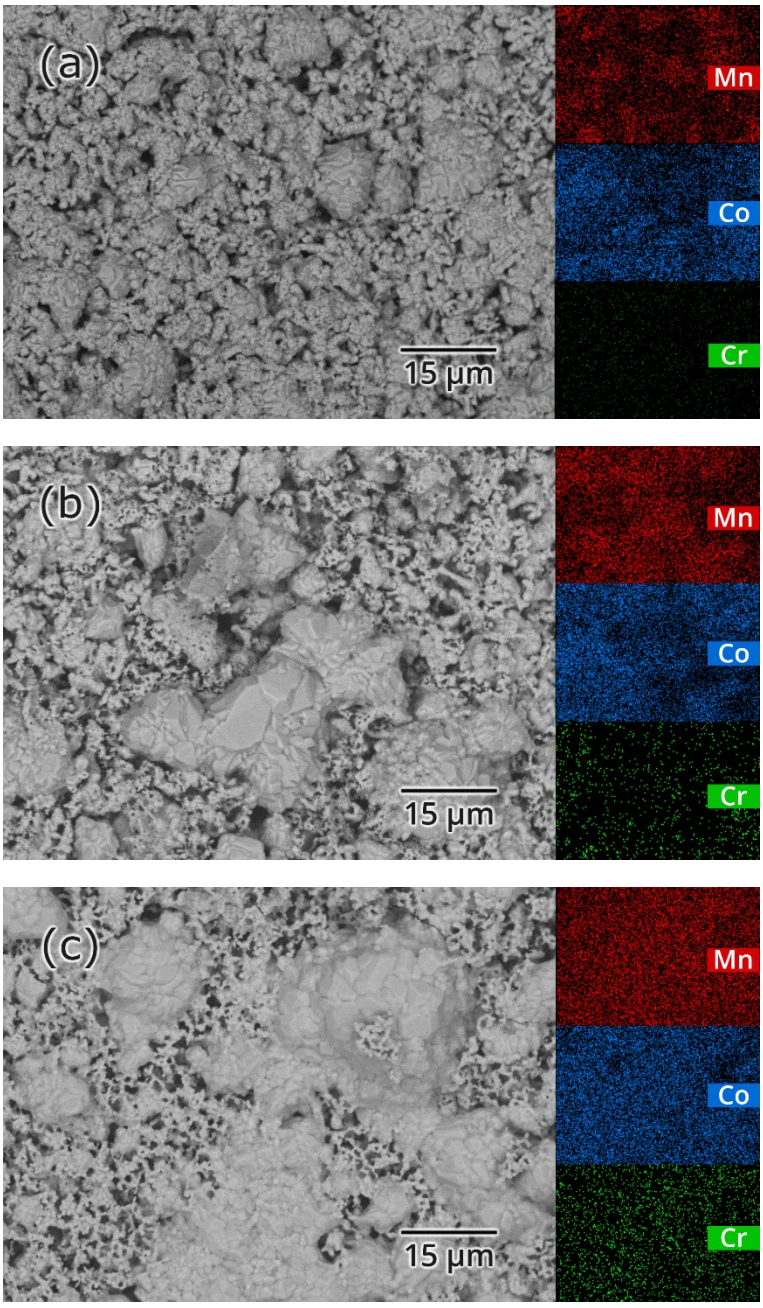

Figure 7. SEM-EDS micrographs of the fractured surface of Co-Mn oxide contact layer (a) as-sintered sample at 800 °C and sample aged at (b) 750 °C and (c) 850 °C for 250 h.

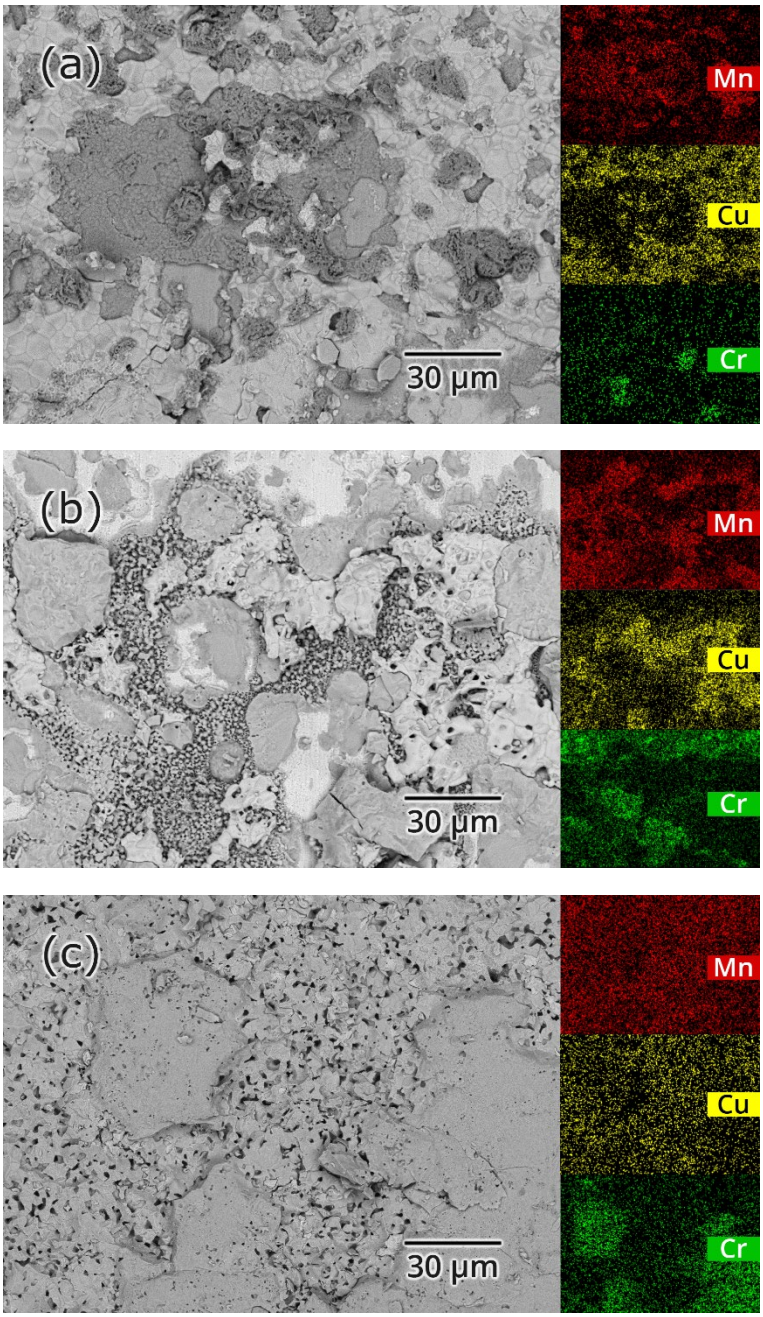

Figure 8. SEM-EDS micrographs of the fractured surface of Cu-Mn oxide contact layer (a) as-sintered sample at 800 °C and sample aged at (b) 750 °C and (c) 850 °C for 250 h.

4 Discussion

The mechanical testing results showed that Cu-Mn contact layer has significantly higher fracture energy than the Co-Mn layer. The fracture energy of the Cu-Mn sample increased after aging, while

for Co-Mn sample, the aging had a negative effect on the mechanical robustness of the layer. The observed difference can be explained on the basis of the XRD and microstructural analyses.

The as-sintered Cu-Mn sample had only one single spinel phase, i.e. $Cu_{1.2}Mn_{1.8}O_4$. Also, the XRD results showed the presence of some metallic Cu. The ductile metallic Cu can contribute to increasing the fracture energy of the sample. As revealed by fractography analysis, the crack propagated partly through the interconnect layer, where ductile Cu particle can accordingly enhance the fracture energy through the well-known crack bridging mechanism. Besides, the SEM images for the Cu-Mn sample show a relatively smooth surface with a higher density in comparison to the Co-Mn sample. A dense layer not only blocks diffusion of oxygen species to oxidize the substrate but also can promote the mechanical properties with enhancing the interconnect/substrate interphase bonding.

On the other hand, the XRD analysis of the as-sintered Co-Mn based sample showed the presence of two spinel phases, namely Co_2MnO_4 (with a cubic structure) and $CoMn_2O_4$ (with a tetragonal structure) and Co_3O_4 phase. The presence of these two Co-Mn spinels is hypothesized to weaken the interface adhesion in the as-sintered sample. The formation of the cubic and tetragonal structures can be assigned to the fact that different oxidation states of Mn (Mn^{2+}, Mn^{3+} and Mn^{4+}) can occupy different lattice sites in a Co-Mn spinel. This high affinity to change in the crystal structure (from tetragonal to cubic and vice-versa), caused by a variation in the oxidation state of Mn (at the aging conditions, i.e. temperature and oxygen partial pressure) can weaken the chemical bonding at the interface of the contact layer and interconnect [5].

More important is perhaps that the Co-Mn spinel is more porous than the Cu-Mn spinel, which is also known to considerably weaken a ceramic material, as the pores acts as a flaws, which can be the nuclei for a crack. Furthermore, the open porosity also allows for oxygen to pass through to coating to a larger extend, which will promote the Cr-oxide scale formation, which could also further weaken the interface.

The Cu-Mn oxide sample aged at 750 °C contained $Cu_{1.2}Mn_{1.8}O_4$ and CuO, while comparatively the sample aged at 850 °C predominantly consisted of $Cu_{1.2}Mn_{1.8}O_4$ and a minor amount of CuO. The CuO in the microstructure can act as a sintering aid and hence can increase the density of the layer upon aging, consequently improving its robustness. It can also block the diffusion path for Cr ions (from interconnects). Furthermore, the CuO can mitigate the structural stability issues caused e.g. by Cu evaporation during long term operation [6], or the ex-solution of Mn cations from spinel structure.

As a result, the increased robustness of the Cu-Mn layer can be explained by the first interdiffusion into the adjacent surfaces and consequent oxidation due to the formation of oxide material from mixed metal precursors, and second due to an increase in the layer density upon aging. However, as seen in D2.6 and D4.1, the Cu tends to “draw” out the Cr enhancing to form Cr, Cu spinels, and thus bringing the Cr evaporation closer to the cell with possible Cr evaporation and poisoning of the cell as a consequence.

5 Conclusion

In this study, Co-Mn and Cu-Mn contact layer materials were deposited on four types of interconnects (AISI 441 and K44M steels, coated and uncoated) using a reactive oxidation bonding approach.

A robust contact layer (with fracture energy of 11.6 J/m^2) was achieved in the Cu-Mn spinel oxide deposited on the CoCe coated AISI 441 stainless steel. Interestingly, the fracture energy of the contact layer increased after aging for 250 h to 15.7 and 19.4 J/m^2, respectively, after aging at the temperature of 750 and 850 °C. The target for improvement of contact layer toughness is 200% over state of the art, being 1.7 J/m^2, i.e. 5.1 J/m^2. With this solution, this target is well achieved. The high fracture energy in Cu-Mn oxide could be due to the enhanced densification of the contact layer and the good bonding between the contact layer and the stainless steel substrate. On the other hand it is known from D2.6 that Cu tends to react with Cr to form Cu,Mn,Cr spinels, and hereby create a transport route for Cr.

The obtained result for the CoMn contact layer only shows long-term fracture energy of 3.3 J/m^2 after aging. However, this is still an improvement over the state of the art of 100%. The higher porosity of this layer is most likely the main source for the lower fracture energy.

Onwards in the project, a combination of the two materials will be investigated to obtain a compromise between mechanical robustness and chemical stability. The combination of the materials can be done either by a layer-wise structuring or by simply mixing the two precursor powders in various amounts. The observed trend in increase in robustness by aging can ensure the long-term mechanical reliability of this system. Complementary studied are ongoing to evaluate the robustness of the layers after aging for 3000 h.

6 Acknowledgements

This project has received funding from the Fuel Cells and Hydrogen 2 Joint Undertaking under grant agreement No 826323. This Joint Undertaking receives support from the European Union's Horizon 2020 research and innovation programme, Hydrogen Europe and Hydrogen Europe research.

References

[1] P.G. Charalambides, H.C. Cao, J. Lund, A.G. Evans, Development of a test method for

measuring the mixed mode fracture resistance of bimaterial interfaces, Mech. Mater. 8 (1990) 269–283. https://doi.org/10.1016/0167-6636(90)90047-J.

[2] I. Hofinger, M. Oechsner, H.-A. Bahr, M. V Swain, Modified four-point bending specimen for determining the interface fracture energy for thin, brittle layers, Int. J. Fract. 92 (1998) 213–220. https://doi.org/10.1023/A:1007530932726.

[3] I. Ritucci, R. Kiebach, B. Talic, L. Han, P. Zielke, P. V. Hendriksen, H.L. Frandsen, Improving the interface adherence at sealings in solid oxide cell stacks, J. Mater. Res. 34 (2019) 1167–1178. https://doi.org/10.1557/jmr.2018.459.

[4] L. Han, B. Talic, K. Kwok, P.V. Hendriksen, H.L. Frandsen, Interface fracture energy of contact layers in a solid oxide cell stack, ACS Appl. Energy Mater. (2020). https://doi.org/10.1021/acsaem.9b02026.

[5] I. Thaheem, D.W. Joh, T. Noh, K.T. Lee, Highly conductive and stable Mn1.35Co1.35Cu0.2Y0.1O4 spinel protective coating on commercial ferritic stainless steels for intermediate-temperature solid oxide fuel cell interconnect applications, Int. J. Hydrogen Energy. 44 (2019) 4293–4303. https://doi.org/https://doi.org/10.1016/j.ijhydene.2018.12.173.

[6] X. Montero, W. Fischer, F. Tietz, D. Stöver, M. Cassir, I. Villarreal, Development and characterization of a quasi-ternary diagram based on La0.8Sr0.2(Co,Cu,Fe)O3 oxides in view of application as a cathode contact material for solid oxide fuel cells, Solid State Ionics. 180 (2009) 731–737. https://doi.org/https://doi.org/10.1016/j.ssi.2009.03.006.